Stock et al. European Radiology Experimental (2025)9:97
https://doi.org/10.1186/s41747-025-00635-5

EUROPEAN SOCIETY OF RADIOLOGY
European Radiology EXPERIMENTAL

ORIGINAL ARTICLE Open Access

Stenosis quantification in high-pitch photon-counting coronary CT angiography: *in vitro* and *in vivo* impact of reconstruction kernel types and sharpness levels

Jonathan Stock[1], Mortiz Halfmann[2], Tilman Emrich[2,3,4*], Lukas Müller[2], Nicola Fink[1], Dirk Graafen[2], Tobias Bäuerle[2], Michaela Hell[5], Martin Geyer[5], Milan Vecsey-Nagy[3], Akos Varga-Szemes[3] and Yang Yang[2]

Abstract

Background We investigated the influence of different kernel types and sharpness levels on *in vitro* and *in vivo* coronary stenosis quantification in high-pitch photon-counting detector coronary CT angiography (PCD-CCTA).

Materials and methods Coronary stenoses were evaluated in a phantom containing two stenosis grades (25% and 50%), and in a retrospective cohort of 30 patients who underwent high-pitch PCD-CCTA. Scans were reconstructed as virtual monoenergetic images at 55 keV using three different kernels (Br, Bv, and Qr) and four sharpness levels (36, 40, 44, and 48). Percent diameter stenosis (PDS) values were compared. *In vitro* measurements were additionally compared with the stenosis reference value. Two readers independently assessed the *in vivo* measurements.

Results *In vitro*, PDS values of all stenoses showed no difference among various kernel types and sharpness levels ($p \geq 0.412$). However, PDS measurements using kernel Bv40 showed the smallest cumulative deviation from the ground truth. *In vivo*, a total of 53 stenoses were identified in 30 patients, aged 63 ± 13 years (mean ± standard deviation), 8/30 (27%) females. There was no significant difference in PDS measurements among reconstructions, either when analyzed per stenosis or stratified by different plaque types ($p = 1.000$). Bv kernels showed higher interobserver reliability (intraclass correlation coefficient: Bv 0.91; Qr 0.88; Br 0.85).

Conclusion With comparable diagnostic accuracy, different kernel types and sharpness levels can be used in high-pitch PCD-CCTA. Due to the *in vivo* advantage in interobserver reliability and the *in vitro* observed lowest cumulative deviation from ground truth, reconstruction with kernel Bv40 should be preferred.

Relevance statement For image reconstruction in PCD-CCTA with high-pitch mode, kernel Bv40 should be considered to obtain the best diagnostic performance and reliability of stenosis quantification.

Key Points

- High-pitch PCD-CCTA images can be reconstructed with different kernels.
- Reconstructions with different kernels showed comparable accuracy on coronary stenosis quantification.
- *In vitro*, Bv40 reconstructions showed superior measurement accuracy to the reference.
- *In vivo*, reconstructions with the Bv kernel had the highest interobserver reliability.
- Reconstruction with kernel Bv40 should be considered in high-pitch PCD-CCTA.

*Correspondence:
Tilman Emrich
Tilman.Emrich@unimedizin-mainz.de
Full list of author information is available at the end of the article

Keywords Computed tomography angiography, Coronary stenosis, Phantoms (imaging), Reproducibility of results, Tomography (x-ray computed)

Graphical Abstract

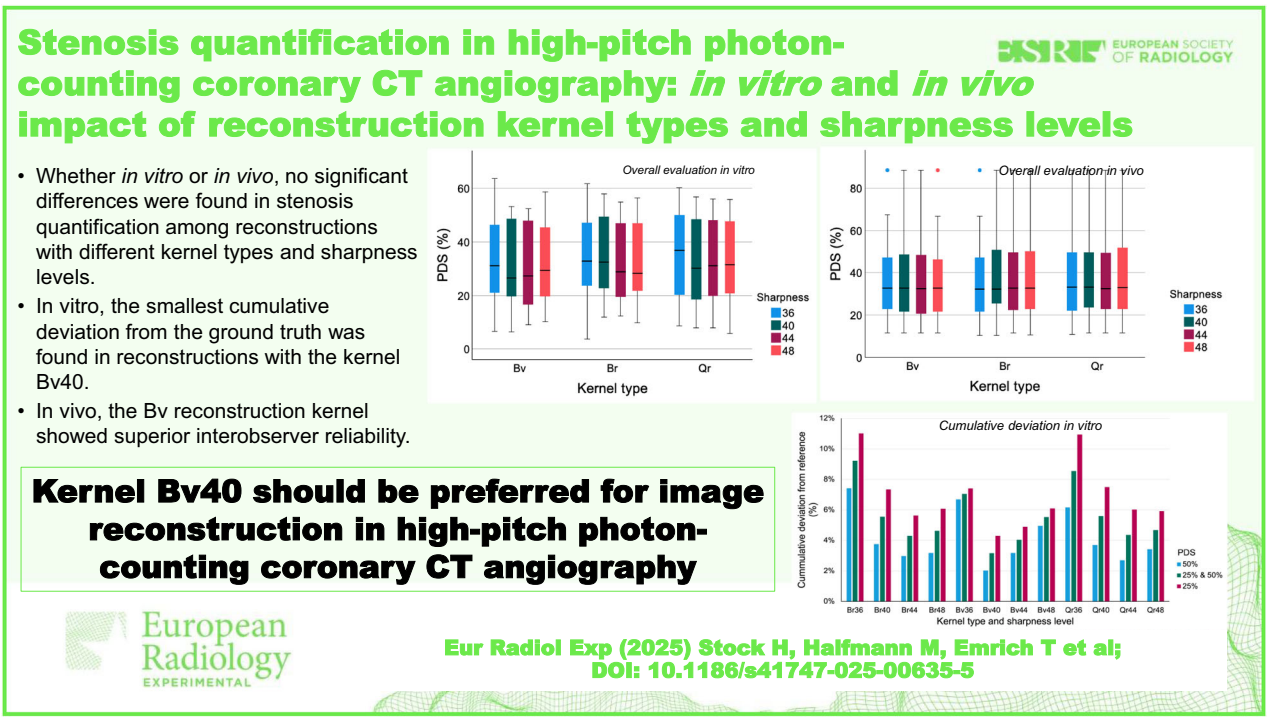

Background

Coronary artery disease (CAD) is the most common heart condition and the leading cause of mortality worldwide [1]. Over the past 20 years, coronary computed tomography angiography (CCTA) has become a well-established noninvasive method for the diagnostic work-up of patients with suspected stable CAD. Due to its excellent sensitivity and high negative predictive value, CCTA is recommended by major international guidelines as the first-line test to rule out obstructive CAD, especially in patients with low to intermediate risk [2–4].

Recently, the first-generation dual-source photon-counting detector (PCD) computed tomography (CT) was introduced and approved for routine clinical use. Compared with conventional energy-integrating detector CT, PCD-CT possesses several advantages, including higher spatial resolution, increased contrast-to-noise ratio, and superior dose efficiency [5–9]. It has the potential to significantly improve the image quality and expand the utility of cardiovascular imaging [10–15].

Advances in PCD-CT reconstruction algorithms are also expected to enhance the accuracy of coronary artery plaque and stenosis quantification [16, 17]. Previous studies investigated the influence of reconstruction kernels and sharpness levels on image quality in high-pitch CCTA [18] and ultra-high-resolution (UHR) CCTA with PCD-CT [19]. *In vitro* and *in vivo* studies indicated that sharper vascular reconstruction kernels improve coronary stenosis quantification and plaque characterization in UHR PCD-CCTA [16, 20]. However, the effects of reconstruction kernels and sharpness levels on stenosis assessment in high-pitch PCD-CCTA, the less dose-intensive alternative to UHR PCD-CCTA for patients with lower pretest probability of CAD, remain unknown.

Therefore, the aim of this study was to investigate the influence of different kernel types and sharpness levels on coronary artery stenosis quantification in high-pitch PCD-CCTA.

Materials and methods

Dynamic vessel phantom

The dynamic vessel phantom included a rod that contained three custom-made vessels with a diameter of 4 mm. The vessels were composed of solid material,

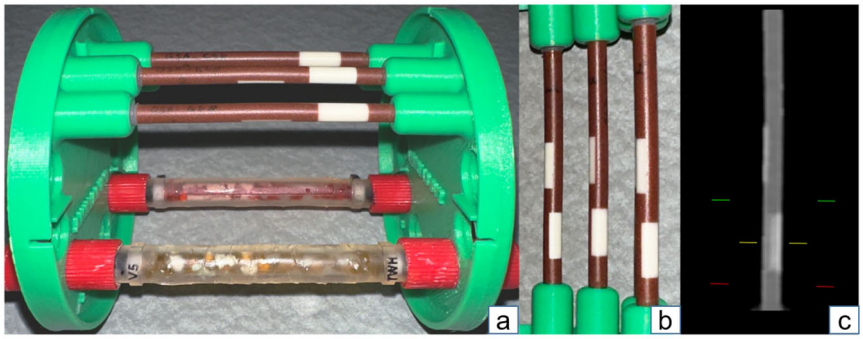

Fig. 1 Custom-made vessel phantom. **a** An assortment of vessel phantoms in a three-dimensional-printed mounting. **b** From left to right: phantom vessel contains 1,000-HU mixed plaques, 1,000-HU calcified plaques, and 800-HU calcified plaques. **c** PCD CT scan of one vessel phantom in coronal reconstruction

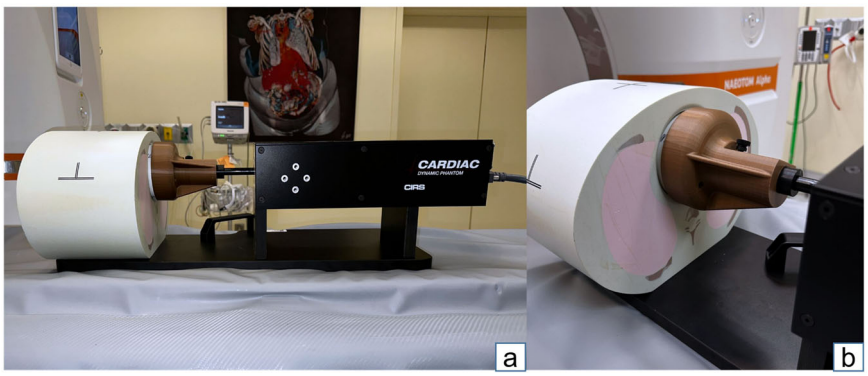

Fig. 2 Dynamic chest phantom. **a** The dynamic chest phantom (CIRS Dynamic Cardiac Phantom, Model 008) comprises an anthropomorphic thorax CT body, moving rod, motion actuator, motion controller, and CIRS Motion Control software. The phantom body contains a fully articulated spine, ribs, and lungs in order to represent the average human thorax in shape, proportion, and composition. **b** A three-dimensional-printed mount affixes the rod that inserts into the thorax phantom and houses the vessel phantoms

mimicking a physiological mixture of iodine contrast medium and blood with an attenuation of 800 HU in one vessel and 1,000 HU in the other two vessels. Each vessel contained two artificial plaques simulating percentage diameter stenosis (PDS) of 25% and 50%. One vessel with 1,000 HU contained mixed plaques, and the other two vessels with 1,000 HU and 800 HU contained calcified plaques (Fig. 1). The rod was mounted in an anthropomorphic chest CT phantom (Fig. 2), which has been described in prior studies [21, 22].

Phantom CT data acquisition

Phantom scans were performed on a first-generation, dual-source CT system (NAEOTOM Alpha, Siemens Healthineers), which contains two photon-counting cadmium telluride detectors with a collimation of 144 × 0.4 mm. The phantom acquisitions used a tube voltage of 120 kVp, a tube current-time product of 100 mAs, a field of view of 200 × 200 mm, and a matrix size of 512 × 512 pixels.

During the image acquisition, heart motion was simulated using a 4D coronary motion simulator with a 10-cm diameter water carrier (Cardio CT Phantom and Sim4D-Cardio, QRM). In combination with an artificial electrocardiographic signal, scanning was performed at 60, 80, and 100 beats per minute with electrocardiographic triggering in the diastole, starting at 70% R–R interval. The phantom scans were repeated five separate times at each heart rate and once more without simulated cardiac motion.

Patient cohort

This retrospective study was approved by the institutional ethics committee (reference number: 2022-16359) with waivers of informed consent and performed in compliance with the Declaration of Helsinki.

Patients who underwent CCTA between February and March 2022 were retrospectively identified based on the following inclusion criteria: (1) CCTA was indicated to exclude or determine CAD, and (2) CCTA was performed with high-pitch "Flash" mode on PCD-CT. Exclusion

criteria were non-evaluable coronary arteries or contraindication to nitroglycerin.

Patient CT data acquisition

Patient scans were performed on the same dual-source PCD system. In the absence of contraindications, patients were administered 0.8 mg sublingual nitroglycerin and a maximum of 10 mg intravenous metoprolol depending on the heart rate. All patients received a dual-bolus injection consisting of 15 mL iodinated contrast agent (Ultravist 370 mgI/mL, Bayer Healthcare) for the test bolus and 70 mL for the main bolus, followed by a saline chaser (25 mL). The electrocardiographic pulsing window was set in the diastole with a start at 60% of the R–R interval. CT scans were acquired at 120 kVp with automated tube current modulation (CARE Dose4D, Siemens Healthineers) in the "Flash-QuantumPlus" mode (pitch factor 3.2, gantry rotation time 0.25 s) with a detector collimation of 144 × 0.4 mm.

Image reconstruction

In vitro reconstructions were performed using a proprietary offline raw data reconstruction platform (ReconCT version 15.0.57554.0, Siemens Healthineers), while *in vivo* reconstructions were processed directly on the PCD-CT system.

In vitro and *in vivo* CT images were reconstructed using three different kernels (Body regular [Br], Body vascular [Bv], and Quantitative regular [Qr]) and four sharpness levels (36, 40, 44, and 48), resulting in a total of 12 reconstructions per CT scan. The image slice thickness was set to 0.4 mm with an increment of 0.2 mm. The vendor-specific level of iterative reconstruction (Quantum iterative reconstruction) was set at the maximum available level (level 3) at the time of the investigation. Virtual monoenergetic images were reconstructed at 55 keV.

Stenosis assessment

In vitro scans were evaluated by a trained reader (J.S.) with 2 years of experience in cardiovascular imaging, under close supervision by a board-certified cardiovascular radiologist (T.E.) with more than 13 years of experience in the field. The analysis of *in vivo* scans was assessed by two readers, one (M.H.) with 5 years of experience and one board-certified cardiovascular radiologist (Y.Y.) with 10 years of experience in cardiovascular imaging.

Stenosis assessment was performed using a commercially available software solution (Syngo.via, Version VB60A, Siemens Healthineers). The CT scans were presented anonymized without image information and in a random order to minimize recall bias. Readers were blinded to kernel, sharpness level, and each other's results. Standard window setting was used with the window level corresponding to the attenuation in the aorta at the level of the left main coronary artery and the window width obtained by multiplying the attenuation by 2.5 [19].

Stenosis quantification was performed on cross-sectional images with vessel diameters measured perpendicular to the vessel centerline. PDS was calculated *in vitro* using the following formula [23]:

$$\mathrm{PDS} = 1 - \frac{D_{\mathrm{stenosis}}}{D_{\mathrm{ref}}}$$

where D_{stenosis} is the minimal lumen diameter within the stenosis and D_{ref} is the average of diameters at the proximal and distal reference points, which were placed at the nearest areas without coronary plaques or wall abnormalities. Since this formula was developed and used for phantom studies with constant vessel diameter and equal distance between stenosis and reference points, a modified formula from Cheng et al, with consideration of the physiological vessel narrowing from proximal to distal segments, was used for *in vivo* stenosis assessment [24]. Accordingly, *in vivo* PDS was calculated using the following formula:

$$\mathrm{PDS} = 1 - \frac{D_{\mathrm{stenosis}}}{D_{\mathrm{prox}} - \left(\frac{X_1}{X_2}\right) * (D_{\mathrm{prox}} - D_{\mathrm{dis}})}$$

where PDS is calculated by interpolation D_{Ref} with reference vessel diameter proximal to the stenosis (D_{prox}), reference vessel diameter distal to the stenosis (D_{dis}), distance between proximal and distal reference sites (X_1), and distance between proximal reference site and stenosis site (X_2) (Fig. 3).

In vivo, the readers also graded plaque types in the stenosis area into calcified, mixed, and noncalcified plaques as previously described [25].

Statistical analysis

Statistical analysis was performed using SPSS (Version 29; IBM Corporation) and GraphPad (Version 8.4.2; GraphPad). The Shapiro–Wilk test was used to test for normal distribution of continuous variables, which were subsequently reported as means with standard deviations or medians with interquartile ranges. Categorial variables are reported as absolute frequencies and respective proportions. Cumulatively averaged deviations between *in vitro* measurements and ground-truth reference are calculated and presented in percent. Different image reconstructions were compared using the Wilcoxon related-samples signed rank test. A two-sided $p < 0.050$ was considered statistically significant. Inter- and intraobserver agreement was evaluated by Cohen's κ and two-way random effects model intraclass correlation coefficients (ICC),

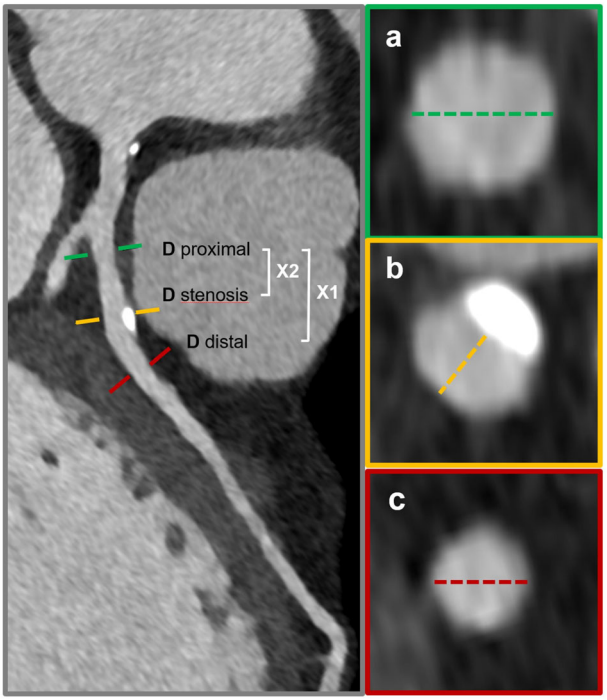

Fig. 3 Assessment of coronary stenosis *in vivo*. Curved multiplanar reconstruction (figure on the left) shows a calcified plaque with proximal left coronary artery narrowing. Vessel diameter at the level of stenosis (**b**, orange line), as well as at the level of the closest unaffected vessel proximal (**a**, green line) and distal to the stenosis (**c**, red line), was measured. The distances along the centerline between the proximal and distal reference sites (between the green and red level, X1) and between the proximal reference site and stenosis site (between the green and orange level, X2) were determined

using the following interpretation: < 0.5 poor, 0.5–0.75 moderate, 0.76–0.9 strong, and > 0.9 excellent agreement [26].

Results

In vitro assessment

In the overall evaluation across all stenoses at different simulated heart rates, there was no difference in PDS measurements among reconstructions with different kernel types and sharpness levels ($p = 0.412$ to 0.990, Fig. 4). In the vessels-based analysis, a significant difference in measured PDS was observed in the vessels with calcified plaques, but not in the vessels with mixed plaques.

Based on cumulative deviation, PDS was closer to the ground-truth reference standard in reconstructions with kernel Bv40 among all reconstruction kernels and sharpness levels, regardless of stenosis grade or plaque composition (Fig. 5).

In the *in vitro* measurement, the intraobserver reliability was excellent (ICC ≥ 0.99).

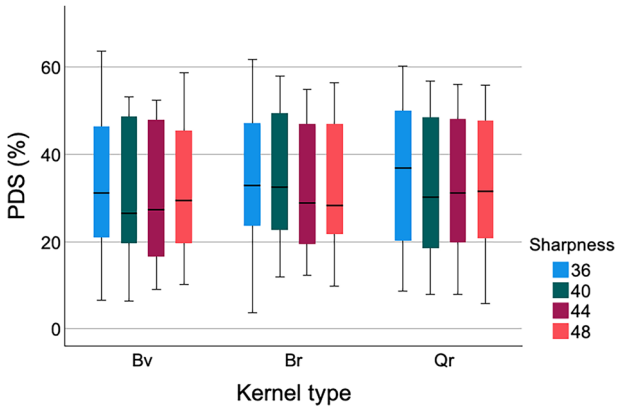

Fig. 4 Overall evaluation *in vitro*. Overall evaluation across all stenoses in the three artificial vessels. Boxplots show PDS value, measured in reconstructions with different kernel types and sharpness levels

Patient characteristics

A total of 34 patients were initially considered for inclusion in the study. Patients were excluded for non-evaluable coronary arteries ($n = 2$) and contraindication to nitroglycerin ($n = 2$). A total of 30 patients (8/30 [27%] females) with a mean age of 63 ± 13 years (range 39–83 years) and a mean body mass index of 25.4 ± 2.98 kg/m^2 were included in the final analysis. The mean heart rate at the time of CT scan was 59 ± 7 beats per minute (Table 1). The mean effective radiation dose was 1.07 ± 0.18 mSv.

Of the 53 coronary stenoses that were identified in the study sample, the majority were caused by calcified plaques (31/53, 58.5%), whereas mixed plaques (14/53, 26.4%) and noncalcified plaques (8/53, 15.1%) were less frequent.

In vivo stenosis assessment

In the per stenosis analysis, the overall median PDS showed no significant difference among the reconstructions with different kernel types and sharpness levels (all p-values Bv, Br, Qr = 1.000) (Fig. 6).

When stratified by plaque type, only slight differences in PDS measurement were observed among different kernel types and sharpness levels, especially in calcified and noncalcified plaques. Overall, there was no evidence of a significant difference between plaque types (all p-values = 1.000) (Fig. 7).

The overall interobserver reliability was strong (ICC ≥ 0.88). Among different kernels, the highest interobserver reliability was found in the reconstructions with the Bv kernel ($ICC_{Bv} \geq 0.91$, $ICC_{Qr} \geq 0.88$, $ICC_{Br} \geq 0.85$).

Discussion

This *in vitro* and *in vivo* study investigated the impact of different reconstruction kernels and sharpness levels on the quantification of coronary artery stenosis in

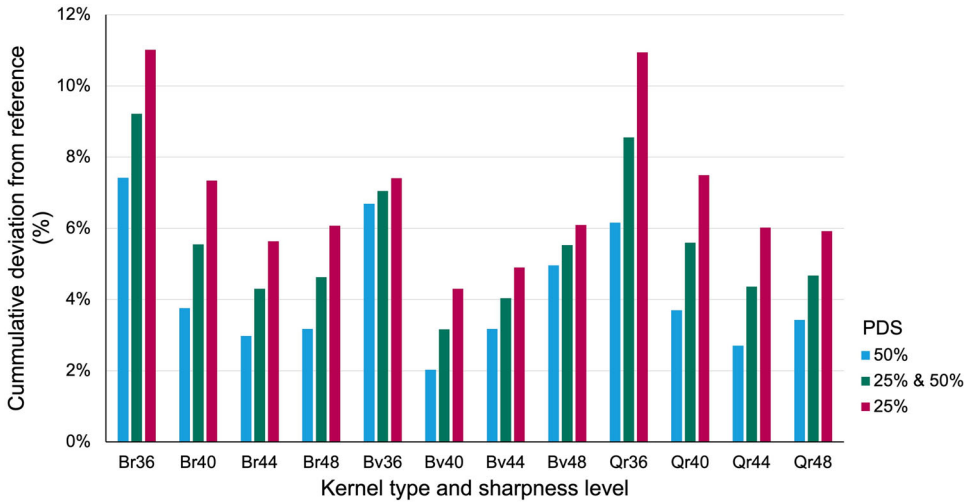

Fig. 5 Cumulative deviation *in vitro*. Cumulative deviation of the measured PDS *in vitro* from the physical reference value in reconstructions with different kernel types and sharpness levels

Table 1 Patient characteristics ($n = 30$)

Age, years	63 ± 13
Sex, male/ female	22 (73%)/8 (27%)
Body mass index, kg/m^2	25.4 ± 3.0
Heart rate, beats per minute	59 ± 7 (range 37–70)
*Radiation dose, mSv	1.07 ± 0.18
CAD-RADS 0	16/30 (54%)
CAD-RADS 1	4/30 (13%)
CAD-RADS 2	3/30 (10%)
CAD-RADS 3	1/30 (3%)
CAD-RADS 4	6/30 (20%)

Data are presented as mean ± standard deviation or *n* (%), unless otherwise specified
CAD-RADS Coronary artery disease-reporting and data system
* Effective dose in mSv was used for radiation dose

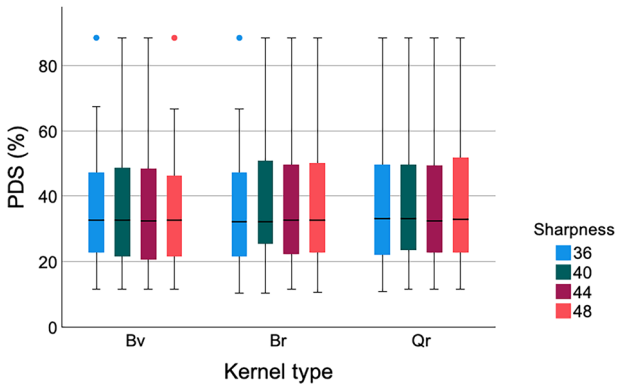

Fig. 6 Overall evaluation *in vivo*. Boxplots show PDS values for *in vivo* stenoses, measured in different reconstructions with different kernel types and sharpness levels

high-pitch PCD-CCTA. The main results are as follows: (1) in both *in vitro* and *in vivo* analysis, there was no significant difference in PDS measurements among different reconstruction kernels and sharpness levels; (2) in the *in vitro* analysis, PDS was measured closer to the ground-truth reference standard in reconstructions with kernel Bv40; and (3) in the *in vivo* study, the highest interobserver reliability for PDS measurements was observed in the reconstructions with the Bv kernels.

CCTA is considered a first-line test for the diagnosis and exclusion of coronary artery stenosis [2–4, 27]. Since the introduction of clinical PCD-CT, the image quality of CCTA has been further improved with increased sharpness, reducing blooming of calcifications, and leading to superior accuracy in stenosis quantification [11, 28]. However, as PCD-CT is a recently introduced technology, only limited literature is available regarding the effect of varying reconstruction parameters for coronary stenosis quantification. To our knowledge, no previous study has systematically evaluated the impact of the convolution kernel and kernel sharpness level on stenosis quantification in high-pitch PCD-CCTA.

In the recently published *in vivo* study, Augustin et al investigated the impact of kernel sharpness level (Bv36/48/56) on image quality, diagnostic confidence, and stenosis quantification in lower extremity PCD-CTA [29]. They found that changing kernel sharpness did not significantly affect the sensitivity and specificity of stenosis assessment. However, the diagnostic concordance of stenosis grading compared with DSA increased significantly with sharper kernels. While our study demonstrated no such observation, it should be noted that the lower

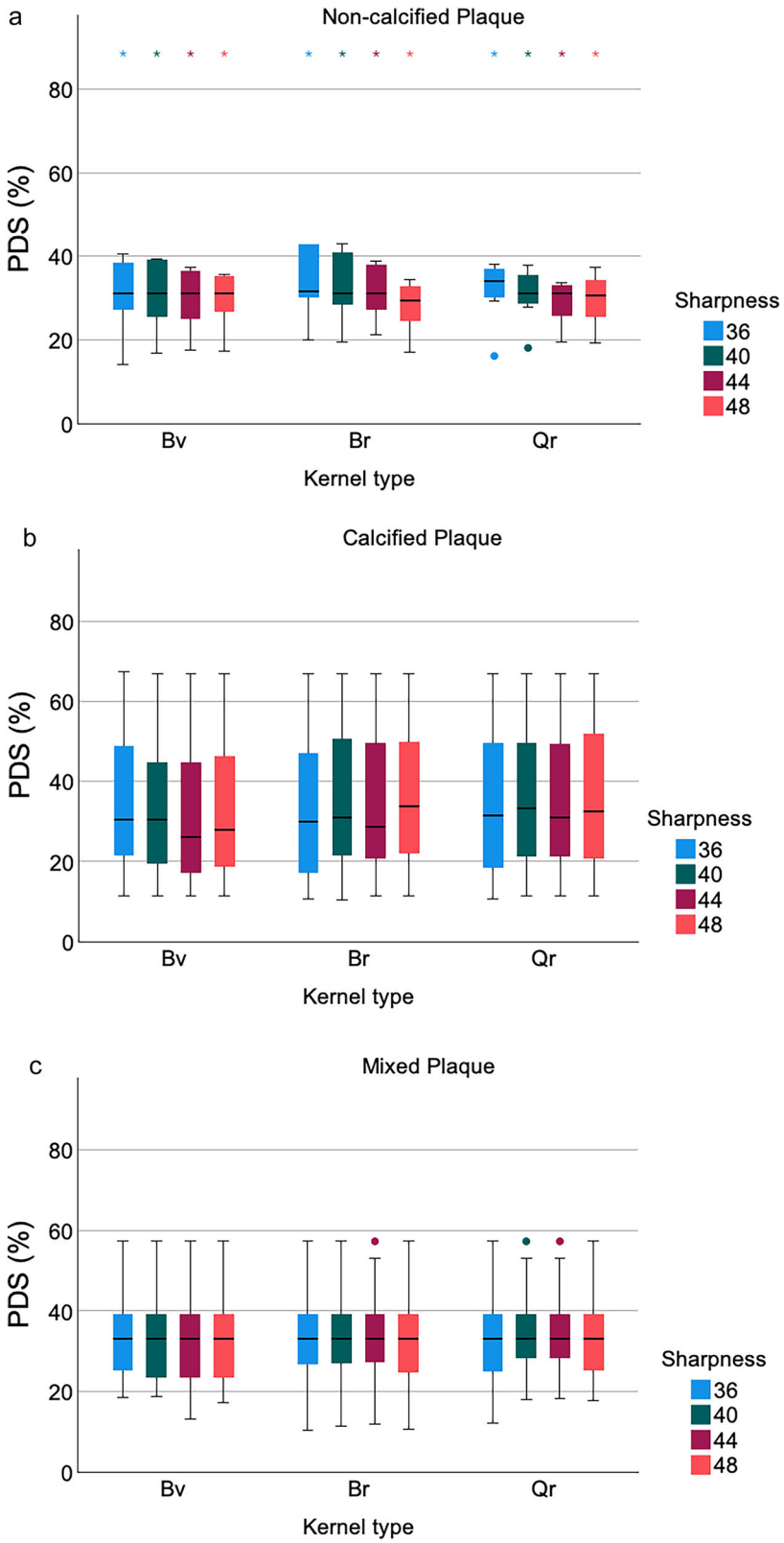

Fig. 7 Evaluation with different plaque types *in vivo*. Boxplots show PDS values stratified by plaque type in reconstructions with different kernel types and sharpness levels: noncalcified, calcified, and mixed plaques (Fig. 7a–c, respectively).

extremity artery scans were performed using spiral acquisitions (*versus* the high-pitch scan mode in our study), and the lower extremity scans were reconstructed with a single vascular kernel. Furthermore, instead of being quantified, lower extremity vessel stenoses were graded on a four-point scale.

Mergen et al [19] reported the influence of kernel sharpness levels on image quality and blooming artefacts in patients with moderate to severe calcium deposits. In their study, PCD-CCTA was performed using the sequential UHR scan mode, and optimal quality for coronary plaque characterization and delineation of adjacent vessel lumen was found in reconstructions using kernel Bv64. Michael et al [30] investigated image quality for cardiac stents in reconstructions with different vascular kernels. In their phantom study, improved image quality to assess the in-stent lumen was found in reconstruction with kernel Bv72. In contrast to our study, CCTAs were performed in UHR scan mode in the above studies. In this scan mode, a higher sharpness level is preferable to exploit the potential of the spatial resolution given by the pixel size [19]. However, in high-pitch mode, the maximum spatial resolution is not directly defined by the pixel size since an interpolation of the raw data is required. This explains the preference for the lower sharpness level, Bv40, in high-pitch scan mode, as shown in our study results.

While the aforementioned studies analyzed the effect of various reconstruction parameters in sequential or UHR PCD-CTA, our study investigated the influence of different kernels and sharpness levels on stenosis quantification in spectral high-pitch PCD-CTA. In our study, there was no significant difference in PDS measurements between different kernels and sharpness levels. However, the highest interobserver reliability in *in vivo* stenosis assessment was found in reconstructions with the vascular (Bv) kernel, and *in vitro* PDS measurements with kernel Bv40 showed the value closest to the reference standard. Taken together with a previous study on image quality [18], our results indicate that kernel Bv40 may be the ideal reconstruction parameter for PCD-CCTA in high-pitch scan mode to achieve accurate stenosis quantification and excellent image quality.

As it is well known, CCTA is a first-line test for the evaluation of patients with suspected CAD, especially in patients with low and intermediate risk. The majority of this CCTA population were patients without relevant stenosis requiring further downstream testing or intervention [31]. Although several studies have reported the benefits of UHR CCTA in reducing calcium blooming and superior accuracy in quantifying coronary stenosis [19, 28, 32–35], there are still some advantages of the high-pitch scan mode. Compared with UHR scan mode, which is likely to suffer from lower *z*-coverage and longer scan duration and may be susceptible to respiratory motion and heart rate variability [19, 33], PCD-CCTA with high-pitch scan mode provides excellent image quality with significantly shorter acquisition time and lower radiation dose [36, 37]. With increasing image quality due to advanced temporal resolution in the third-generation dual-source CT [38] and the higher photon efficiency of PCD [39], the threshold above which heart rate begins to affect diagnostic quality is also increasing in PCD-CCTA with high-pitch scan mode [40–42]. Considering the above aspects, our result is particularly useful for patients with low and intermediate pretest probabilities and patients with low coronary calcium burden, who need CCTA to exclude significant CAD.

The following limitations merit consideration. First, in the *in vitro* study, only two stenosis grades, two plaque types (calcified and mixed plaques), at three simulated heart rates were investigated. Second, the *in vivo* analysis included a limited number of patients undergoing PCD-CCTA to exclude or detect CAD in a single center. Third, there was no physical reference for *in vivo* measurements, since almost all patients were not indicated for subsequent invasive coronary angiography. Finally, in this study, we investigated only the impact of different kernels and sharpness levels on coronary artery stenosis quantification. The effects of other reconstruction parameters, such as quantum iterative reconstruction or keV levels, should be evaluated in future studies.

In conclusion, image reconstruction with different kernel types and with sharpness levels between 36 and 48 can be used in high-pitch CCTA on PCD-CT with comparable diagnostic accuracy. Due to its better interobserver reliability *in vivo* and its closest measurements to the ground-truth reference *in vitro*, together with the results of a previous study on image quality, reconstruction with the Bv40 kernel should be preferred.

Abbreviations

Br	Body regular
Bv	Body vascular
CAD	Coronary artery disease
CCTA	Coronary computed tomography angiography
CT	Computed tomography
PCD	Photon-counting detector
PDS	Percentage diameter stenosis
Qr	Quantitative regular
UHR	Ultra-high-resolution

Acknowledgements

We acknowledge that, in this manuscript, no large language models or other generative artificial intelligence software were used.

Author contributions

JS: conceptualization, investigation, methodology, analysis, data interpretation, and visualization. MHa: conceptualization, software, analysis, data interpretation, visualization, and writing—review and editing. TE:

conceptualization, data interpretation, project administration, supervision, and writing—review and editing. LM: conceptualization and data curation. DG: data curation, software, and writing—review and editing. TB: conceptualization, project administration, and supervision. MHe: conceptualization and resources. MG: conceptualization and resources. MV-N: methodology, resources, and software. AV-S: conceptualization, methodology, project administration, resources, supervision, and writing—review and editing. YY: conceptualization, investigation, project administration, analysis, data interpretation, visualization, and writing—original draft. All authors approved the final manuscript and agreed with the submission.

Funding
Open Access funding enabled and organized by Projekt DEAL.

Data availability
The datasets used and/or analyzed during the current study are available from the corresponding author on reasonable request.

Declarations

Ethics approval and consent to participate
This retrospective study was approved by the institutional ethics committee (reference number: 2022-16359) with waivers of informed consent and performed in compliance with the Declaration of Helsinki.

Consent for publication
The requirement of informed consent was waived by the institutional ethics committee.

Competing interests
TE receives speaker fee, institutional research-/ travel support from Siemens Healthineers, is an advisory board member from Siemens Healthineers, and a consultant from Circle Cardiovascular Imaging. YY, MHa, and DG receive institutional research support from Siemens Healthineers. AV-S receives institutional research support and/or personal fees from Bayer, Elucid, and Siemens Healthineers. TE, DG, and MVN are members of the Scientific Editorial Board of *European Radiology Experimental* (Section Editor: Computed Tomography, member Computer Tomography section, member Cardiovascular section, respectively). AV-S is Deputy Editor of *European Radiology Experimental*. As such, these authors did not participate in the selection or review processes for this article. The remaining authors declare that they have no competing interests.

Author details
[1]Department of Radiology, Ludwig Maximilian University Hospital, Munich, Germany. [2]Department of Diagnostic and Interventional Radiology, University Medical Center Mainz, Mainz, Germany. [3]Division of Cardiovascular Imaging, Department of Radiology and Radiological Science, Medical University of South Carolina, Charleston, SC, USA. [4]Deutsches Zentrum für Herz-Kreislauf-Forschung (DZHK), Berlin, Germany. [5]Department of Cardiology, University Medical Center Mainz, Mainz, Germany.

Received: 26 March 2025 Revised: 24 July 2025 Accepted: 4 September 2025
Published online: 24 September 2025

References
1. Malakar AK, Choudhury D, Halder B, Paul P, Uddin A, Chakraborty S (2019) A review on coronary artery disease, its risk factors, and therapeutics. J Cell Physiol 234:16812–16823. https://doi.org/10.1002/jcp.28350
2. Gulati M, Levy PD, Mukherjee D et al (2021) 2021 AHA/ACC/ASE/CHEST/SAEM/SCCT/SCMR guideline for the evaluation and diagnosis of chest pain: executive summary: a report of the American College of Cardiology/American Heart Association Joint Committee on Clinical Practice Guidelines. Circulation 144:e368–e454. https://doi.org/10.1161/CIR.0000000000001030
3. Moss AJ, Williams MC, Newby DE, Nicol ED (2017) The updated NICE guidelines: cardiac CT as the first-line test for coronary artery disease. Curr Cardiovasc Imaging Rep 10:15. https://doi.org/10.1007/s12410-017-9412-6
4. Knuuti J, Wijns W, Saraste A et al (2020) 2019 ESC guidelines for the diagnosis and management of chronic coronary syndromes. Eur Heart J 41:407–477. https://doi.org/10.1093/eurheartj/ehz425
5. Gutjahr R, Halaweish AF, Yu Z et al (2016) Human imaging with photon counting-based computed tomography at clinical dose levels: contrast-to-noise ratio and cadaver studies. Invest Radiol 51:421–429. https://doi.org/10.1097/RLI.0000000000000251
6. Rajagopal JR, Farhadi F, Solomon J et al (2021) Comparison of low dose performance of photon-counting and energy integrating CT. Acad Radiol 28:1754–1760. https://doi.org/10.1016/j.acra.2020.07.033
7. Yu Z, Leng S, Kappler S et al (2016) Noise performance of low-dose CT: comparison between an energy integrating detector and a photon counting detector using a whole-body research photon counting CT scanner. J Med Imaging 3:043503. https://doi.org/10.1117/1.JMI.3.4.043503
8. Symons R, Reich DS, Bagheri M et al (2018) Photon-counting computed tomography for vascular imaging of the head and neck: first *in vivo* human results. Invest Radiol 53:135–142. https://doi.org/10.1097/RLI.0000000000000418
9. Sartoretti T, McDermott M, Mergen V et al (2023) Photon-counting detector coronary CT angiography: impact of virtual monoenergetic imaging and iterative reconstruction on image quality. Br J Radiol 96:20220466. https://doi.org/10.1259/bjr.20220466
10. Pinos D, Griffith J 3rd, Emrich T et al (2023) Intra-individual comparison of image quality of the coronary arteries between photon-counting detector and energy-integrating detector CT systems. Eur J Radiol 166:111008. https://doi.org/10.1016/j.ejrad.2023.111008
11. Flohr T, Schmidt B, Ulzheimer S, Alkadhi H (2023) Cardiac imaging with photon counting CT. Br J Radiol 96:20230407. https://doi.org/10.1259/bjr.20230407
12. Soschynski M, Hagen F, Baumann S et al (2022) High temporal resolution dual-source photon-counting CT for coronary artery disease: Initial multicenter clinical cxperience. J Clin Med. https://doi.org/10.3390/jcm11206003
13. Gnasso C, Pinos D, Schoepf UJ et al (2024) Impact of reconstruction parameters on the accuracy of myocardial extracellular volume quantification on a first-generation, photon-counting detector CT. Eur Radiol Exp 8:70. https://doi.org/10.1186/s41747-024-00469-7
14. Tremamunno G, Varga-Szemes A, Schoepf UJ et al (2024) Intraindividual reproducibility of myocardial radiomic features between energy-integrating detector and photon-counting detector CT angiography. Eur Radiol Exp 8:101. https://doi.org/10.1186/s41747-024-0
15. Wolf EV, Muller L, Schoepf UJ et al (2023) Photon-counting detector CT-based virtual monoenergetic reconstructions: repeatability and reproducibility of radiomics features of an organic phantom and human myocardium. Eur Radiol Exp 7:59. https://doi.org/10.1186/s41747-023-00371-8
16. Halfmann MC, Bockius S, Emrich T et al (2024) Ultrahigh-spatial-resolution photon-counting detector CT angiography of coronary artery disease for stenosis assessment. Radiology 310:e231956. https://doi.org/10.1148/radiol.231956
17. Zsarnoczay E, Fink N, Schoepf UJ et al (2024) Accuracy of ultra-high resolution and virtual non-calcium reconstruction algorithm for stenosis evaluation with photon-counting CT: results from a dynamic phantom study. Eur Radiol Exp 8:102. https://doi.org/10.1186/s41747-024-00482-w
18. Yang Y, Fink N, Emrich T et al (2023) Optimization of kernel type and sharpness level improves objective and subjective image quality for high-pitch photon counting coronary CT angiography. Dianostics (Basel) 13:1937
19. Mergen V, Sartoretti T, Baer-Beck M et al (2022) Ultra-high-resolution coronary CT angiography with photon-counting detector CT: feasibility and image characterization. Invest Radiol 57:780–788. https://doi.org/10.1097/RLI.0000000000000897
20. Mergen V, Eberhard M, Manka R, Euler A, Alkadhi H (2022) First in-human quantitative plaque characterization with ultra-high resolution coronary photon-counting CT angiography. Front Cardiovasc Med 9:981012. https://doi.org/10.3389/fcvm.2022.981012

21. Achenbach S, Delgado V, Hausleiter J, Schoenhagen P, Min JK, Leipsic JA (2012) SCCT expert consensus document on computed tomography imaging before transcatheter aortic valve implantation (TAVI)/transcatheter aortic valve replacement (TAVR). J Cardiovasc Comput Tomogr 6:366–380. https://doi.org/10.1016/j.jcct.2012.11.002
22. Wolf EV, Halfmann MC, Varga-Szemes A et al (2024) Photon-counting detector CT virtual monoenergetic images for coronary artery stenosis quantification: phantom and *in vivo* evaluation. AJR Am J Roentgenol 222:e2330481. https://doi.org/10.2214/AJR.23.30481
23. Allmendinger T, Nowak T, Flohr T et al (2022) Photon-counting detector CT-based vascular calcium removal algorithm: assessment using a cardiac motion phantom. Invest Radiol 57:399–405. https://doi.org/10.1097/RLI.0000000000000853
24. Cheng V, Gutstein A, Wolak A et al (2008) Moving beyond binary grading of coronary arterial stenoses on coronary computed tomographic angiography: insights for the imager and referring clinician. JACC Cardiovasc Imaging 1:460–471. https://doi.org/10.1016/j.jcmg.2008.05.006
25. Hadamitzky M, Achenbach S, Al-Mallah M et al (2013) Optimized prognostic score for coronary computed tomographic angiography: results from the CONFIRM registry (COronary CT angiography evaluatioN For clinical outcomes: an InteRnational Multicenter registry). J Am Coll Cardiol 62:468–476. https://doi.org/10.1016/j.jacc.2013.04.064
26. Koo TK, Li MY (2016) A guideline of selecting and reporting intraclass correlation coefficients for reliability research. J Chiropr Med 15:155–163. https://doi.org/10.1016/j.jcm.2016.02.012
27. Group DT, Maurovich-Horvat P, Bosserdt M et al (2022) CT or invasive coronary angiography in stable chest pain. N Engl J Med 386:1591–1602. https://doi.org/10.1056/NEJMoa2200963
28. Koons E, VanMeter P, Rajendran K, Yu L, McCollough C, Leng S (2022) Improved quantification of coronary artery luminal stenosis in the presence of heavy calcifications using photon-counting detector CT. Proc SPIE Int Soc Opt Eng 12031:120311A
29. Augustin AM, Hartung V, Grunz JP et al (2024) Photon-counting detector CT angiography versus digital subtraction angiography in patients with peripheral arterial disease. Acad Radiol 31:2973–2986. https://doi.org/10.1016/j.acra.2024.02.008
30. Michael AE, Schoenbeck D, Becker-Assmann J et al (2023) Coronary stent imaging in photon counting computed tomography: optimization of reconstruction kernels in a phantom. Eur J Radiol 166:110983. https://doi.org/10.1016/j.ejrad.2023.110983
31. Winther S, Nissen L, Westra J et al (2019) Pre-test probability prediction in patients with a low to intermediate probability of coronary artery disease: a prospective study with a fractional flow reserve endpoint. Eur Heart J Cardiovasc Imaging 20:1208–1218. https://doi.org/10.1093/ehjci/jez058
32. Zsarnoczay E, Fink N, Schoepf UJ et al (2023) Ultra-high resolution photon-counting coronary CT angiography improves coronary stenosis quantification over a wide range of heart rates—a dynamic phantom study. Eur J Radiol 161:110746. https://doi.org/10.1016/j.ejrad.2023.110746
33. Si-Mohamed SA, Boccalini S, Lacombe H et al (2022) Coronary CT angiography with photon-counting CT: first-in-human results. Radiology 303:303–313. https://doi.org/10.1148/radiol.211780
34. Hagar MT, Soschynski M, Saffar R et al (2023) Accuracy of ultrahigh-resolution photon-counting CT for detecting coronary artery disease in a high-risk population. Radiology 307:e223305. https://doi.org/10.1148/radiol.223305
35. Emrich T, Hell M (2023) Plaque composition on ultra-high-resolution coronary computed tomography angiography with optical coherence tomography correlation. Eur Heart J 44:1765. https://doi.org/10.1093/eurheartj/ehac560
36. Finck T, Klambauer K, Hendrich E, Will A, Martinoff S, Hadamitzky M (2021) Radiation dose and image quality of a high-pitch prospective spiral first approach in coronary computed tomography angiography (CCTA). J Cardiovasc Dev Dis. https://doi.org/10.3390/jcdd8100119.
37. Seppelt D, Kolb C, Kuhn JP et al (2019) Comparison of sequential and high-pitch-spiral coronary CT-angiography: image quality and radiation exposure. Int J Cardiovasc Imaging 35:1379–1386. https://doi.org/10.1007/s10554-019-01568-y
38. Lin CT, Chu LCH, Zimmerman SL, Fishman EK (2020) High-pitch non-gated scans on the second and third generation dual-source CT scanners: comparison of coronary image quality. Clin Imaging 59:45–49. https://doi.org/10.1016/j.clinimag.2019.09.008
39. Willemink MJ, Persson M, Pourmorteza A, Pelc NJ, Fleischmann D (2018) Photon-counting CT: technical principles and clinical prospects. Radiology 289:293–312. https://doi.org/10.1148/radiol.2018172656
40. Malone LJ, Olson A, Barker AJ, Mong DA, Weinman JP, Browne LP (2020) Visualization of proximal coronary arteries on high-pitch electrocardiogram-triggered computed tomography in pediatric congenital heart disease: effects of heart rate and body surface area. Pediatr Radiol 50:1375–1380. https://doi.org/10.1007/s00247-020-04730-0
41. Rotkopf LT, Froelich MF, Riffel P et al (2023) Influence of heart rate and heart rate variability on the feasibility of ultra-fast, high-pitch coronary photon-counting computed tomography angiography. Int J Cardiovasc Imaging. https://doi.org/10.1007/s10554-023-02808-y.
42. Morsbach F, Gordic S, Desbiolles L et al (2014) Performance of turbo high-pitch dual-source CT for coronary CT angiography: first ex vivo and patient experience. Eur Radiol 24:1889–1895. https://doi.org/10.1007/s00330-014-3209-7

Publisher's Note